

# Tumor-associated macrophages promote the metastasis and growth of non-small-cell lung cancer cells through NF- $\kappa$ B/PP2Ac-positive feedback loop

Zhan-Wen Liang<sup>1</sup> | Xin-Xin Ge<sup>1</sup> | Meng-Dan Xu<sup>1</sup> | Hualong Qin<sup>2</sup> | Meng-Yao Wu<sup>1</sup> | Meng Shen<sup>1</sup> | Yan Zhang<sup>1</sup> | Xiao-Meng Liu<sup>1</sup> | Kai Chen<sup>1</sup> | Wei Li<sup>1</sup> | Weiming Duan<sup>1</sup> | Songbing Qin<sup>3</sup>

<sup>1</sup>Department of Oncology, The First Affiliated Hospital of Soochow University, Suzhou, China

<sup>2</sup>Department of Cardiothoracic Surgery, The First Affiliated Hospital of Soochow University, Suzhou, China

<sup>3</sup>Department of Radiation Oncology, The First Affiliated Hospital of Soochow University, Suzhou, China

## Correspondence

Meng-Dan Xu and Weiming Duan, Department of Oncology, the First Affiliated Hospital of Soochow University, Suzhou, China.

Emails: mengdanxu@suda.edu.cn (M-DX) and wmduan@suda.edu.cn (WD)

Songbing Qin, Department of Radiation Oncology, the First Affiliated Hospital of Soochow University, Suzhou 215006, China. Email: qin92244@163.com

## Funding information

the Project of Invigorating Health Care through Science, Technology and Education, Jiangsu Provincial Medical Youth Talent, Grant/Award Number: QNRC2016709

## Abstract

Non-small-cell lung cancer (NSCLC), with its aggressive biological behavior, is one of the most diagnosed cancers. Tumor-associated inflammatory cells play important roles in the interaction between chronic inflammation and lung cancer, however the mechanisms involved are far from defined. In the present study, by developing an orthotopic NSCLC mouse model based on chronic inflammation, we proved that an inflammatory microenvironment accelerated the growth of orthotopic xenografts *in vivo*. Tumor-associated macrophages, the most abundant population of inflammatory cells, were identified. Treatment with macrophage-conditioned medium (MCM) promoted the growth and migration of NSCLC cells. Using bioinformatics analysis, we identified downregulated PP2Ac expression in NSCLC cells upon treatment with MCM. We further confirmed that this downregulation was executed in an NF- $\kappa$ B pathway-dependent manner. As I $\kappa$ B kinase (IKK) has been proved to be a substrate of PP2Ac, inhibition on PP2Ac could result in amplification of NF- $\kappa$ B pathway signaling. Overexpression of PP2Ac, or the dominant-negative forms of IKK or I $\kappa$ B, attenuated the acceleration of growth and metastasis by MCM. Using bioinformatics analysis, we further identified that CXCL1 and COL6A1 could be downstream of NF- $\kappa$ B/PP2Ac pathway. Luciferase assay and ChIP assay further confirmed the location of response elements on the promoter regions of CXCL1 and COL6A1. Elevated CXCL1 facilitated angiogenesis, whereas upregulated COL6A1 promoted proliferation and migration.

## KEYWORDS

COL6A1, CXCL1, non-small-cell lung cancer, protein phosphatase 2A, tumor-associated macrophages

Zhan-Wen Liang, Xin-Xin Ge, Meng-Dan Xu and Hualong Qin contributed equally to this work.

This is an open access article under the terms of the Creative Commons Attribution-NonCommercial-NoDerivs License, which permits use and distribution in any medium, provided the original work is properly cited, the use is non-commercial and no modifications or adaptations are made.

© 2021 The Authors. *Cancer Science* published by John Wiley & Sons Australia, Ltd on behalf of Japanese Cancer Association.

## 1 | INTRODUCTION

The incidence of lung cancer among all cancers is the second highest with rates of 14% and 13% in males and females respectively.<sup>1</sup> Non-small-cell lung cancer (NSCLC) is the most common type of cancer affecting the lungs accounting for approximately 85% of all lung cancer cases.<sup>1-3</sup> NSCLC is a highly invasive tumor with the characteristics of dysregulation of apoptosis, uncontrolled cell proliferation, invasion, angiogenesis, and metastasis.<sup>4,5</sup> Despite the recent advances in lung cancer researches, the 5-y survival rate of patients with NSCLC is still only c. 18%.<sup>1</sup>

Clinical epidemiological studies showed a strong correlation between chronic inflammation and cancer.<sup>4,6,7</sup> In addition, 20% of cancers are associated with chronic infections.<sup>8</sup> Recently, a variety of studies have demonstrated a close connection between inflammatory infiltration and the development of lung cancer.<sup>5</sup> However, the mechanisms involved are still far from being defined.

Inflammatory cells play an important role in the interaction between chronic inflammation and lung cancer.<sup>9</sup> Inflammatory cells provide multifunctional molecules into the tumor microenvironment, including growth factors, pro-angiogenic factors, and extracellular matrix-modifying enzymes, which can maintain proliferative signals or restrict apoptosis, promote angiogenesis, invasion, epithelial-mesenchymal transition (EMT) activation, and metastasis.<sup>10-12</sup>

A previous study has demonstrated that, in the presence of macrophage-conditioned medium (MCM), breast cancer cells became detached and acquired an EMT-like morphology, which occurred during metastasis.<sup>13</sup> Macrophages, which are the major population of tumor-associated inflammatory cells, have 2 distinct phenotypes: M1 and M2.<sup>14</sup> M1 is associated with a better prognosis of NSCLC and is related to anti-tumor behaviors.<sup>15</sup> M2, also termed as tumor-associated macrophages (TAMs),<sup>16</sup> is the most common phenotype that promotes tumor growth, angiogenesis, invasion, and metastasis.<sup>15</sup> TAMs are prominent type of inflammatory cells in many tumors and can infiltrate tumors at an early stage of cancer development. Previous studies have demonstrated that TAMs can promote the growth and metastasis of cancer cells.<sup>13,17</sup>

In the present study, using *in vivo* and *in vitro* models, we investigated the mechanisms involved in the progression of NSCLC driven by TAMs.

## 2 | MATERIALS AND METHODS

### 2.1 | Patients and tissue samples

The study material was obtained from 58 patients with lung cancer whose tissue samples were available (mean age 57 y, range 32-78 y) and who were treated between January 2010 and July 2017 at the First Affiliated Hospital of Soochow University. All human tissue samples were obtained and handled in accordance with an approved Institutional Review Board application (the Committee on Medical Ethics, the First Affiliated Hospital of Soochow University).

Patients received systemic therapy in accordance with National Comprehensive Cancer Network lung cancer clinical practice guidelines and were followed regularly. Prognostic analyses were performed regarding overall survival (OS).

### 2.2 | Reagents

TGF- $\beta$ , IL-6, IL-8, and CXCL1 were purchased from PeproTech. Okadaic acid (OA), SP600125, PD98059, GF109203X, Bay-11-7082, and BIRB796 were purchased from Enzo Life Science International. IL-4 was purchased from PeproTech. TGF- $\beta$  neutralizing antibody (MAB1835, R&D Systems), IL-6 neutralizing antibody (MAB206, R&D Systems), IL-1b neutralizing antibody (MAB601, R&D Systems) were purchased from R&D Systems.

### 2.3 | Immunohistochemistry

All resection specimens were fixed in 10% buffered formalin and paraffin embedded by routine processing. Sections were obtained at 3- $\mu$ m thickness, heated at 60°C for 30 min, deparaffinized, and hydrated through a series of xylene and alcohol baths before staining. The slides were microwaved with antigen retrieval solution (citrate buffer, pH 6.0, containing 0.3% trisodium citrate and 0.04% citric acid) for 5 min. After replenishment of the solution, the slides were microwaved again for 5 min and then allowed to cool for 20 min. The sections were then rinsed in PBS and immersed in 3% H<sub>2</sub>O<sub>2</sub> for 15 min to block endogenous peroxidase. Thereafter, the sections were incubated with 10% BSA at room temperature for 60 min to block nonspecific antibodies. Immunohistochemical staining was performed with rabbit anti-CD163 antibody (ab87099; Abcam), rabbit anti-Ki67 antibody (ab15580; Abcam), rabbit anti-CD34 antibody (ab81289; Abcam), rabbit anti-PP2Ac antibody (ab32141; Abcam), or rabbit anti-phosphorylated IKK (S176, ab138426; Abcam) at room temperature for 1 h. After 20-min incubation with the corresponding secondary antibodies, the bound complex was visualized using a SuperPicture Polymer Detection kit (no. 87-8963; Invitrogen).

### 2.4 | Microvessel density (MVD) evaluation

Angiogenesis vascularity was defined as the number of vessels per field counted in the area of highest vascular density, termed as microvessel density (MVD). Endothelial cells were marked with anti-CD34 antibody. CD34 antigen was localized in the cytoplasm and cellular membrane of vascular endothelial cells. Single endothelial cells, endothelial cell clusters, and microvessels in the tumors, clearly separated from adjacent microvessels, were counted. Peritumoral vascularity and vascularity in areas of necrosis were not scored. A vascular lumen was not a requirement for a structure to be counted as a microvessel. Branching structures were counted as 1, unless there was a break in the continuity of the

vessel, in which case it was counted as 2 distinct vessels. Areas with a higher density of CD34<sup>+</sup> cells and cell clusters relative to adjacent areas were classified as 'hot spots.' The slides were initially screened at low power to identify the areas with the highest number of microvessels or vascularity hot spots. Microvessels were counted in  $\times 400$  magnification fields. MVD was defined as the number of manually counted vessel profiles per mm<sup>2</sup> taken as the average from the 3 hot-spot counts.

## 2.5 | Orthotopic xenograft nude mouse model

Here, 4-wk-old female BALB/c athymic nude mice (SLAC Laboratory Animal Co. Ltd, Shanghai, China) were maintained in a specific room that was climate controlled, with food and water, and on a 12 h/12 h, light/dark cycle. Mice were allowed to adapt to the housing facilities for 7 d before any experimental procedures were begun. All protocols were approved by the animal use and care committee of Soochow University. Chronic pneumonia was established by injection of porcine pancreatic elastase (PPE). PPE (Solarbio) was dissolved in 0.9% normal saline. The mice were anesthetized and an incision of the neck skin was made. Then 3.75 units of PPE in 50  $\mu$ L solvent was injected into the main trachea.

At 2 wk after PPE injection, NSCLC cells ( $5 \times 10^6$ ) in 100  $\mu$ L Matrigel (Becton Dickinson) were injected into the left lungs of nude mice. At 5 wk later, the mice were anesthetized and given D-luciferin in PBS. At 20 min after D-luciferin injection, bioluminescence was imaged with a charge-coupled device camera (IVIS; Lumina II, PerkinElmer). Then, the lung and tumor tissues were stripped, formalin fixed, and paraffin embedded.

## 2.6 | Subcutaneous xenograft nude mouse model

NSCLC cells were injected subcutaneously into nude mice in a total volume of 100  $\mu$ L ( $5 \times 10^6$  cells) and the mice were assigned doxycycline (4 mg/mL) treatment, which was conducted twice a week. At the end of the experiment, the mice were anesthetized. Then, the tumors were resected, formalin fixed, and paraffin embedded.

## 2.7 | Cells culture

The human NSCLC cell lines H292 and H1650, and the human monocytic leukemia cell line THP-1 were purchased from the ATCC. Cells were maintained in RPMI-1640 medium (Gibco). Medium was supplemented with 10% FBS (Gibco), 100 U/mL penicillin, and 100 mg/mL streptomycin at 37°C in a 5% CO<sub>2</sub> in air incubator with a humidified atmosphere. The cells were passaged every 2-3 d to maintain exponential growth. Mouse macrophage RAW264.7 cells were purchased from the ATCC and were maintained in DMEM (Gibco). Medium and culture conditions were the same as described earlier.

## 2.8 | Macrophage preparation and culture

THP-1 cells were seeded and cultured in RPMI-1640 medium supplemented with 160 nmol/L PMA and 10% FBS. After 24 h, activated macrophage-like THP-1 cells were further cultured in medium supplemented with 40 ng/mL human macrophage colony-stimulating factor (MCSF; PeproTech Inc). Cells were allowed to differentiate for 7 d in the presence of MCSF. On day 7, fresh medium without MCSF was added to the cells, and the cells were cultured for another 48 h. The culture medium was collected, centrifuged, stored in aliquots at -80°C, and defined as MCM. RAW264.7 were seeded and cultured in DMEM medium supplemented with 10 ng/mL IL-4 and 10% FBS. After 24 h, fresh medium without IL-4 was added to the cells, and the cells were cultured for another 48 h. The culture medium was collected, centrifuged, stored in aliquots at -80°C, and defined as mouse MCM.

## 2.9 | Methyl thiazolyl tetrazolium (MTT) assay

Cells growth was evaluated using an MTT assay. Briefly,  $5 \times 10^4$  cells per well were inoculated onto 24-well plates. After treatments for various periods of time, MTT (Sigma) was added to each well at a final concentration of 0.5 mg/mL. The mixture was incubated at 37°C for 6 h. The medium was then removed, and 800  $\mu$ L DMSO (Sigma) was added to each well. Absorbance was measured at 490 nm using a microplate reader (Thermo Fisher Scientific). Relative cell viability was calculated as follows: relative cell viability = (mean absorbance of the test wells/mean absorbance of the control wells)  $\times$  100%.

## 2.10 | Wound healing assay

Cells ( $1 \times 10^4$ /well) were seeded into 6-well plates and grown to confluency. The monolayer culture was artificially scraped wounded with a sterile micropipette tip to create a denuded zone of constant width. Each well was washed with PBS twice to remove the detached cells. Cell migration to the wounded region was observed using an XDS-1B inverted microscope (MIC Optical and Electrical Instrument, Chongqing, China) and photographed ( $\times 40$  magnification). Images were captured at 0, 4, 8, 12, 16, 20 and 24 h to monitor the wound healing process. The wound areas were measured using ImageJ software (NIH).

## 2.11 | Bioinformatics analysis

The enrichment of immune cell subpopulations was analyzed in 19 solid tumors using a web-accessible relational database TCIA (<https://tcia.at/>), which provided the results of comprehensive immunogenomic analyses of next-generation sequencing (NGS) data. Macrophages and others immune cell types were identified using single sample Gene Set Enrichment Analysis (ssGSEA) and the

deconvolution method, to determine the expression of predefined immune subsets that were overrepresented in the tumor microenvironment. The gene expression profiles GSE9315 found after MCM treatment in NSCLC cells were retrieved from the GEO database (<https://www.ncbi.nlm.nih.gov/geo/>) for analysis. The selection criterion was defined as a more than 1.5-fold difference in the level of expression. A heat map of differentially expressed genes (DEGs) was generated using the online tool Functional Enrichment Analysis Tool (FunRich) (<http://www.funrich.org/>). The Database for Annotation, Visualization, and Integrated Discovery (DAVID) (<https://david.ncifcrf.gov/>) and FunRich were used to annotate input genes, classify gene functions, identify gene conversions, and carry out Gene Ontology (GO) term analysis. The Kyoto Encyclopedia of Genes and Genomes (KEGG) pathway database (<http://www.genome.jp/kegg/pathway.html>) was used for pathway analysis and mapping. A *P* value < .05 was set as the cut-off criterion. Assessment and integration of protein-protein interactions (PPI) were performed using the STRING database (<http://string-db.org/>). A combined score > 0.4 was set as the cut-off criterion. The network constructed by STRING was visualized using Cytoscape software (<http://cytoscape.org/>).

## 2.12 | Western blot analysis

Total protein was extracted using a lysis buffer containing 50 mmol/L Tris-HCl (pH 7.4), 150 mmol/L NaCl, 1% Triton X-100, 0.1% sodium dodecyl sulfate (SDS), 1 mmol/L EDTA, protease inhibitors (10 mg/mL leupeptin, 10 mg/mL aprotinin, 10 mg/mL pepstatin A, 1 mmol/L 4-[2-aminoethyl] benzenesulfonyl fluoride), and phosphatase inhibitors (1 mmol/L NaF, 1 mmol/L Na<sub>3</sub>VO<sub>4</sub>). Protein extracts were separated using 10% SDS-polyacrylamide gel electrophoresis (PAGE) and were transferred to nitrocellulose filter (NC) membranes. After 1 h blocking in 5% non-fat milk, the membranes were incubated overnight at 4°C with rabbit anti-PP2Ac antibody (ab32141; Abcam), rabbit anti-phosphorylated IKK antibody (Ser 176/180, Cell Signaling Technology), rabbit anti-IKK antibody (Cell Signaling Technology), mouse anti-phospho-IκB antibody (Ser 32/36, Cell Signaling Technology), rabbit anti-IκB antibody (Cell Signaling Technology), or mouse anti-β-actin antibody (Santa Cruz Biotechnologies). Protein expression was determined using horseradish peroxidase-conjugated antibodies followed by ECL (Millipore) detection. β-Actin was used as the internal control.

## 2.13 | Real-time PCR

Total RNA was extracted using TRIzol reagent (Invitrogen) in accordance with the manufacturer's protocol. After spectrophotometric quantification, 1 μg total RNA in a final volume of 20 μL was used for reverse transcription with PrimeScript RT Reagent kit (TaKaRa) in accordance with the manufacturer's protocol. Aliquots of cDNA corresponding to equal amounts of RNA were used for quantification of mRNA by real-time PCR using the Light Cycler

96 Real-time Quantitative PCR Detection system (Roche). The reaction system (13 μL) contained the corresponding cDNA, forward and reverse primers, and the SYBR Green PCR master mix (Roche). All data were analyzed using B2M gene expression as an internal standard. The specific primers were as follows: B2M, forward, 5'-TCAAGAAGGTGGTGAAGCAG-3', reverse, 5'-AAGGTGGAGGAGTGGGTGTC-3', product, 112 bp; PP2Ac $\alpha$ , forward, 5'-CGC CAGAAGTACACGAGGAAC-3', reverse, 5'-CGTTGGATTCTTTTGT CAGGATTT-3', product, 240 bp; PP2Ac $\beta$ , forward, 5'-GGGAAACCT GCCTTTGTAT-3', reverse, 5'-CATCATTAGTATGGCACATTTGGTC-3', product, 156 bp; PP2Ac, forward, 5'-GTTACCAAGGAGCTGG ACCA-3', reverse, 5'-CATGCACATCTCCACAGACAGTAAC-3', product, 164 bp; CXCL1, forward, 5'-CACCCAAAGAACATCCAAAGT-3', reverse, 5'-CCTTCAGGAACAGCCACCA-3', product, 210 bp; COL 6A1, forward, 5'-ATCTTCGTGGTGGTGGTCATAA-3', reverse, 5'-TG GAGGACAGGGTTTGGTG-3', product, 354 bp. F4/80, forward, 5'-CTTCTGCTGTGCTGCTGTT-3', reverse, 5'-GCCGTCTGGTT GTCAGTCTTGT-3', product, 123 bp. CD86, forward, 5'-GGTCACA GCAGAAGCAGCCAAA-3', reverse, 5'-TTCAGAGGAGCAGCACCA GAGA-3', product, 102 bp. CD163, forward, 5'-CTGGACTGTGGCG TGGCAATT-3', reverse, 5'-GCTTCGTGGTCAGCCTCAGAG-3', product, 212 bp.

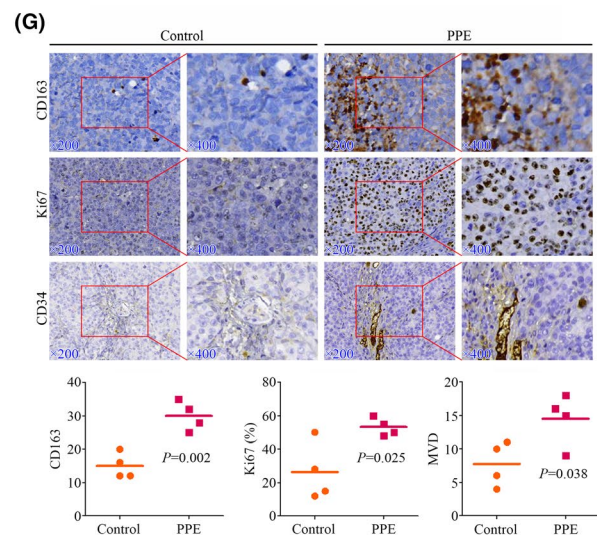
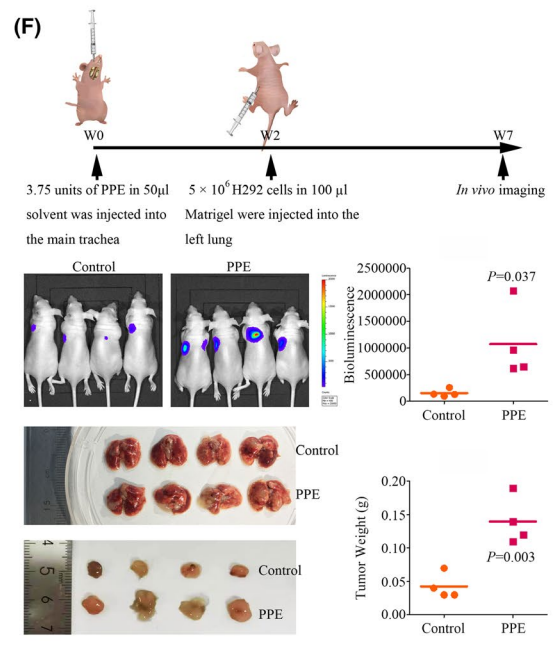
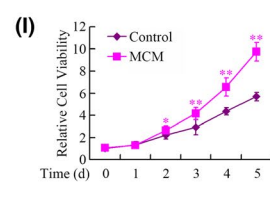
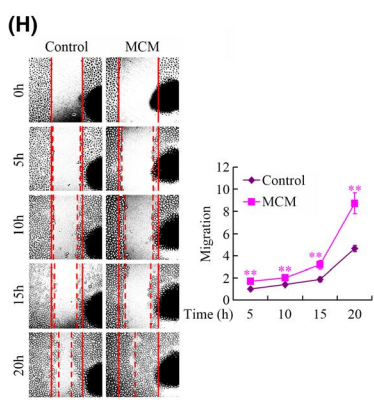
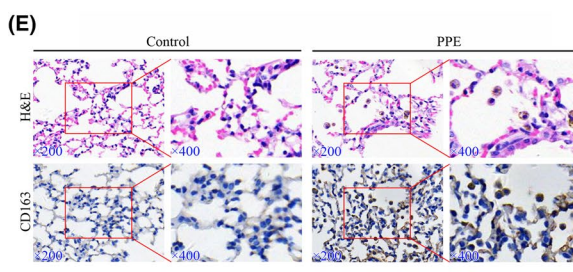
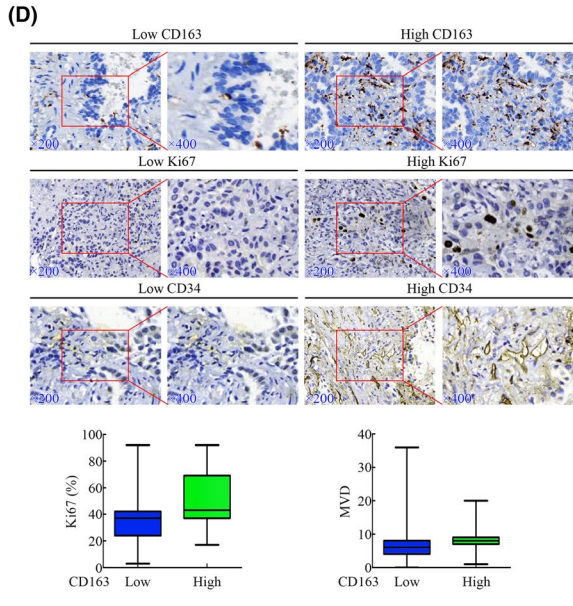
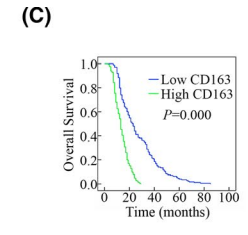
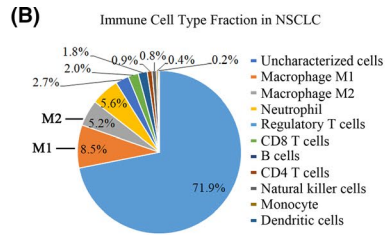
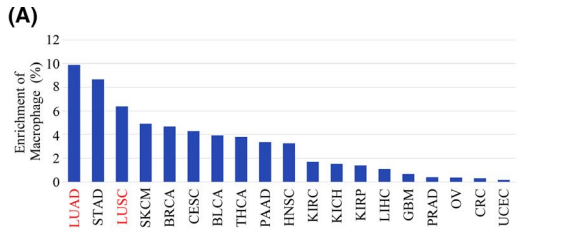
## 2.14 | Construction of overexpression plasmid and lentivirus preparation

A lentiviral Tet-ON advanced inducible expression system was used for doxycycline (Dox)-dependent gene regulation and contained a regulator vector pLVX-Tet-On Advanced and a response vector pLVX-Tight-Puro (provided by Shanghai Taitool Bioscience Co. Ltd.). Vectors containing coding sequences (CDS) of a dominant-negative mutant form of IKK $\alpha$  (DN-IKK $\alpha$ , S176/180A), a dominant-negative mutant form of IκB $\alpha$  (DN-IκB $\alpha$ , S32/36A), and wild-type PP2Ac $\alpha$  (WT-PP2Ac $\alpha$ ) have been described previously (PMID: 21376459, PMID: 21958460).<sup>18,19</sup> The CDSs were PCR amplified and subcloned into the response vector pLVX-Tight-Puro. To produce separate regulator and response lentiviral supernatants, HEK293T cells and the Lenti-X HTX Packaging System were used to generate high-titer lentiviral supernatants from the pLVX-Tet-On Advanced Vector and from the pLVX-Tight-Puro Vector, which contained the gene of interest, following the protocol in the Lentiviral Packaging Kit (Cat. No. 632162, Clontech Laboratories, Inc). Target cells were then simultaneously co-transfected with the 2 lentiviruses. After culturing for 48-72 h, the cells are harvested for analysis.

## 2.15 | RNA interference and generation of stably knockdown cell lines

The sequences of small hairpin RNAs (shRNAs) against human CXCL1 (①. 5'-GCGGAAAGCTTGCCTCAAT-3', ②. 5'-GATGCTGAAC AGTGACAAA-3', ③. 5'-GGTATGATTAACCTCTACCT-3', ④. 5'-GCAC





and PPE treatment and an orthotopic xenograft nude mouse model. H&E staining and immunohistochemistry confirmed the infiltration of M2 into the lung (Figure 1E), suggesting successful establishment

of a nude mouse model of orthotopic pneumonia. We found that the tumors in the PPE group were larger than in the control group (Figure 1F), and the expression levels of both Ki67 and MVD were

**FIGURE 1** TAMs promoted the progression of NSCLC both in vitro and in vivo. A, Enrichment of macrophage across 19 solid cancers, including lung adenocarcinoma (LUAD), stomach adenocarcinoma (STAD), lung squamous cell carcinoma (LUSC), skin cutaneous melanoma (SKCM), breast invasive carcinoma (BRCA), cervical squamous cell carcinoma and endocervical adenocarcinoma (CESC), bladder urothelial carcinoma (BLCA), thyroid carcinoma (THCA), pancreatic adenocarcinoma (PAAD), head and neck squamous cell carcinoma (NHSC), kidney renal clear cell carcinoma (KIRC), kidney chromophobe (KICH), kidney renal papillary cell carcinoma (KIRP), liver hepatocellular carcinoma (LIHC), glioblastoma multiforme (GBM), prostate adenocarcinoma (PRAD), ovarian serous cystadenocarcinoma (OV), colorectal cancer (CRC), uterine corpus endometrial carcinoma (UCEC). B, The mean fraction of immune subpopulations in NSCLC. C, Kaplan-Meier curves for OS based on tumor CD163 expression in patients with NSCLC. D, Immunohistochemical examinations of CD163, Ki67, and CD34 levels in human NSCLC tissue samples, and the quantitative relationships between the expression levels of CD163 and Ki67/MVD. \* $P < .05$  and \*\* $P < .01$  compared with the control groups. E, H&E staining and immunohistochemical examinations of CD163 in mice chronic pneumonia samples established by PPE treatment. F, Establishment of a nude mouse chronic pneumonia model by PPE treatment and orthotopic xenograft model by H292 cells. Representative in vivo bioluminescence images and bioluminescence analysis of lung orthotopic xenografts. Photographs of orthotopic xenografts and tumor weight in the PPE group vs the control group. G, Immunohistochemical examination of CD163, Ki67 and CD34 levels in mice H292 orthotopic xenografts after PPE treatment, and the quantitative expression levels of CD163, Ki67, and MVD analyzed by SPSS. H, MCM treatment resulted in time-dependent inhibition on the migration of H292 cells by wound healing assay. \*\* $P < .01$  compared with the control groups. I, MCM treatment resulted in time-dependent growth inhibition of H292 cells by MTT. \* $P < .05$  and \*\* $P < .01$  compared with the control groups

higher (Figure 1G), indicating that M2 infiltration into the tumor microenvironment significantly elevated the growth and angiogenesis of lung cancer. We also found that mouse M2-type macrophages could induce human tumor cell migration in vitro (Figure S2B).

In addition, to investigate the role of TAMs in lung cancer in vitro, we used MCM to pretreat lung cancer cells. We discovered that TAMs could promote proliferation and migration of lung cancer cells (Figure 1I,H).

### 3.2 | Downregulation of PP2Ac by TAMs participated in the progression of NSCLC

To verify the molecular mechanisms involved in the effects of TAMs during the progression of lung cancer, bioinformatics analysis was performed based on the microarray GSE9315, downloaded from the GEO database (<https://www.ncbi.nlm.nih.gov/geo/>), this contained the gene data for NSCLC cells with or without treatment with MCM. In total, 176 DEGs were identified in LUAD cells, and consisted of 29 upregulated and 147 downregulated genes (Figure S1A). In addition, to gain further insight into the functions of the DEGs, we performed functional enrichment analysis with the DAVID and KOBAS bioinformatics resources to explore the underlying biological function. GO term analysis was used to show the biological process and molecular functions of DEGs. Meanwhile, a PPI network of DEGs was constructed using Cytoscape software (<http://cytoscape.org/>). We found that 176 DEGs were significantly enriched in ECM-receptor interaction, P13K-Akt, TNF, TGF-beta, MAPK, NF- $\kappa$ B, and p53 signaling pathway (Figure S1B-G). In addition, as shown in Figure 2A, PP2Ac $\beta$  was downregulated in the PPI network of DEGs, this was consistent with our previous study in pancreatic cancer.<sup>25</sup>

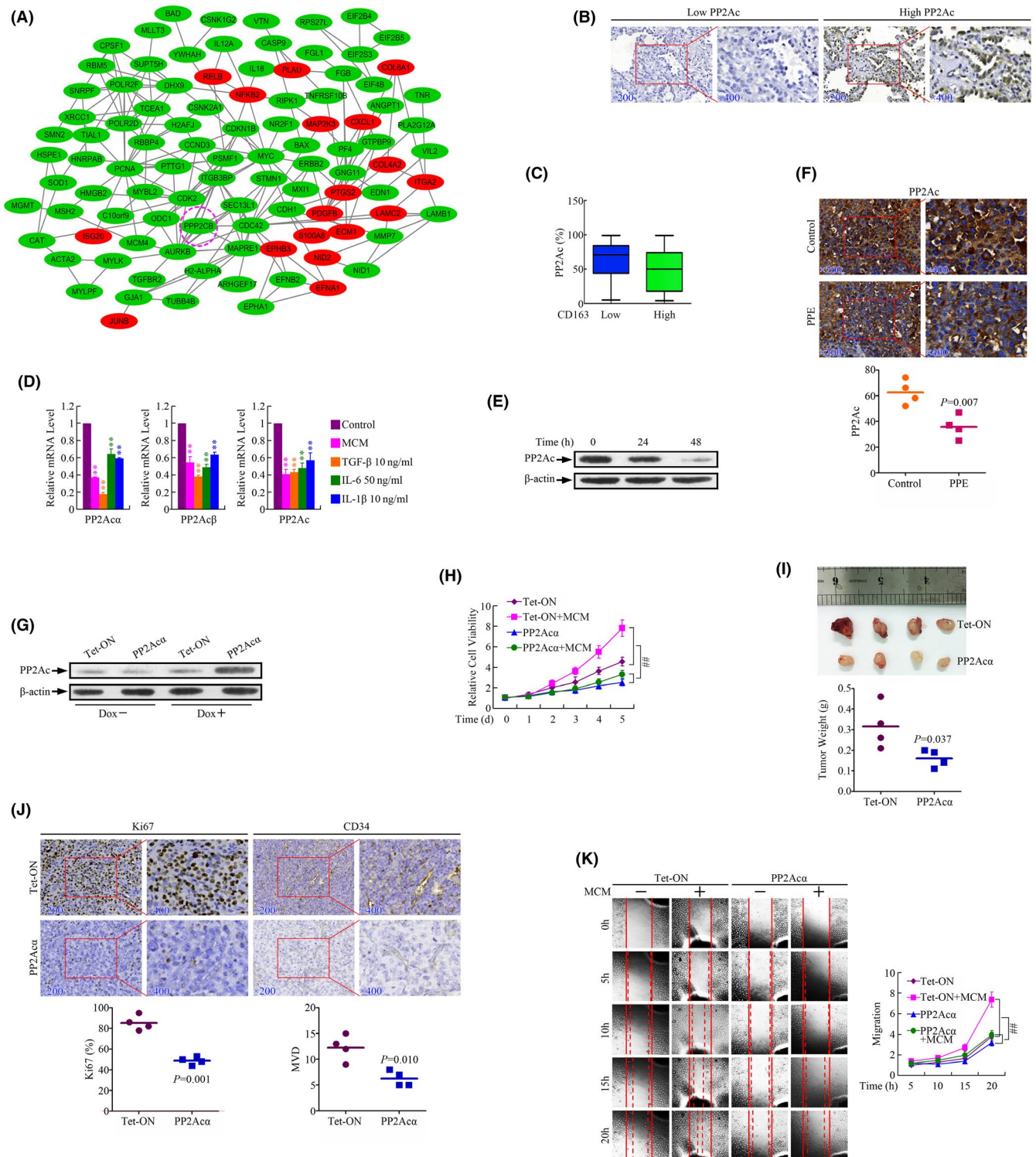
To further investigate the role of PP2Ac in NSCLC, we firstly detected the expression of PP2Ac in samples from patients with NSCLC using immunohistochemistry (Figure 2B), and found that the expression of PP2Ac was negatively correlated with CD163 (Figure 2C). TGF- $\beta$ , IL-6, and IL-1 $\beta$  were the main cytokines secreted from TAMs.<sup>26</sup> PP2Ac contains 2 subunits,  $\alpha$  and  $\beta$ , and their major

sequence has 97% identity.<sup>27</sup> To verify the impact of these factors on PP2Ac, we then detected the expression levels of PP2Ac, PP2Ac $\alpha$  and PP2Ac $\beta$  following treatment with MCM, TGF- $\beta$ , IL-6 and IL-1 $\beta$ . As expected, all of these cytokines could downregulate the expression of PP2Ac and its subunits (Figure 2D). We also performed experiments with neutralizing antibodies antagonizing TGF- $\beta$  (10  $\mu$ mol/L), IL-6 (3  $\mu$ g/mL), and IL-1 $\beta$  (10  $\mu$ g/mL) in MCM to observe the expression of PP2Ac in cancer cells. As shown in Figure S2C, we found that inhibition of TGF- $\beta$ , IL-6, and IL-1 $\beta$  attenuated the downregulation of PP2Ac, PP2Ac $\alpha$  and PP2Ac $\beta$ . Western blot analysis further confirmed that the level of PP2Ac was decreased after cell treatment with MCM in vitro (Figure 2E). We also detected the expression of PP2Ac in the specimens of NSCLC orthotopic xenografts after PPE treatment, and found that the expression of PP2Ac was negatively correlated with PPE treatment (Figure 2F).

To explore whether PP2Ac participated in the process of TAM-induced NSCLC progression, PP2Ac $\alpha$  was overexpressed in the H292 cell line through a lentiviral Tet-ON advanced inducible expression system (Figure 2G). We found that overexpression of PP2Ac $\alpha$  impaired the proliferation and migration of lung cells induced by treatment with MCM in vitro (Figure 2H,K). Moreover, overexpression of PP2Ac also significantly weakened the growth and angiogenesis of tumors in subcutaneous xenograft nude mouse models (Figure 2I,J). Therefore, the pro-tumor effects of TAMs in the microenvironment may be executed through mechanisms involving downregulation of the expression of PP2Ac.

### 3.3 | TAMs accelerated the progression of NSCLC through a NF- $\kappa$ B/PP 2Ac positive feedback loop

Our previous study found that the NF- $\kappa$ B pathway is an important upstream pathway regulating the expression of PP2Ac in pancreatic cancer.<sup>25</sup> I $\kappa$ B kinase (IKK), the key regulator of the NF- $\kappa$ B pathway, is one of the direct substrates of PP2A.<sup>28,29</sup> Based on the classical NF- $\kappa$ B pathway cascade, activated IKK can induce sequential phosphorylation of I $\kappa$ B at Ser 32 and 36, which subsequently causes I $\kappa$ B



to be ubiquitinated and degraded in a proteasome-dependent manner, resulting in the release and nuclear translocation of the NF- $\kappa$ B complex.<sup>30</sup> In this study, we found using bioinformatics analysis that the NF- $\kappa$ B pathway was also involved in the process of TAM-induced progression of lung cancer (Figure S1G). Therefore, we supposed that TAMs accelerated the progression of lung cancer by repressing the expression of PP2Ac, which then might cause activation of the NF- $\kappa$ B pathway through phosphorylation of IKK.

To verify this hypothesis, we then detected the expressions of p-IKK in the specimens from patients with NSCLC by immunohistochemistry and found that the expression of p-IKK was positively related to CD163 but negatively associated with PP2Ac (Figure 3B). Similar results were found in the specimens of NSCLC orthotopic xenografts after PPE treatment. As shown in Figure 2C, the expression of p-IKK was also positively correlated with PPE treatment.

**FIGURE 2** Downregulation of PP2Ac by TAMs participated in the progression of NSCLC. A, Protein-protein interactions (PPI) network of differentially expressed genes (DEGs). B, Immunohistochemical examinations of PP2Ac levels in human NSCLC tissue samples. C, The quantitative relationships between the expression levels of PP2Ac and CD163.  $**P < .01$  compared with the control groups. D, The mRNA levels of PP2Ac $\alpha$ , PP2Ac $\beta$  and PP2Ac in H292 cells after treatment with MCM, TGF- $\beta$  (10 ng/mL), IL-6 (50 ng/mL) and IL-1 $\beta$  (10 ng/mL) by real-time PCR.  $**P < .01$  compared with the control groups. E, The protein levels of PP2Ac in H292 cells after treatment with MCM by western blot. F, Immunohistochemical examinations of PP2Ac levels in H292 orthotopic xenografts samples after treatment with PPE, and the quantitative expression levels of PP2Ac analyzed by SPSS. G, Confirmation of overexpression of PP2Ac $\alpha$  in H292 cells based on a lentiviral Tet-ON advanced inducible expression system by western blot. H, MTT confirmed that the overexpression of PP2Ac $\alpha$  impaired the time-dependent proliferation of H292 cells induced by MCM.  $##P < .01$  compared with the control groups. I, Photographs of subcutaneous xenografts and tumor weight in the H292 PP2Ac $\alpha$  overexpression group vs the control group. J, Immunohistochemical examination of Ki67 and CD34 levels in subcutaneous xenografts samples upon overexpression of PP2Ac $\alpha$ , and the quantitative relationships between the expression levels of PP2Ac $\alpha$  and Ki67/MVD. K, Wound healing assay confirmed that overexpression of PP2Ac $\alpha$  impaired the time-dependent inhibition of migration of H292 cells induced by MCM.  $##P < .01$  compared with the control groups

In addition, as shown by western blot in Figure 3D, treatment with MCM induced phosphorylation of IKK and I $\kappa$ B with a consistent abatement of the total protein level of I $\kappa$ B and resulted in the activation of the NF- $\kappa$ B pathway. EF-24 (IKK inhibitor) and Bay 11-7082 (I $\kappa$ B inhibitor) could both inhibit the NF- $\kappa$ B pathway. We found that inhibition of the NF- $\kappa$ B pathway could weaken the inhibitory effects of TAMs on PP2Ac at both mRNA and protein levels (Figure 3E,F). Moreover, we also established DN-IKK $\alpha$  (S176/180A) and DN-I $\kappa$ B $\alpha$  (S32/36A) overexpression cell lines through a Tet-ON advanced inducible expression system and found that overexpression of DN-IKK $\alpha$  (S176/180A) and DN-I $\kappa$ B $\alpha$  (S32/36A) could impair the inhibitory effects of TAMs on PP2Ac at both mRNA and protein levels (Figure 3E,F). Similar results were confirmed upon treatment with TGF- $\beta$ , IL-6 and IL-1 $\beta$ , the main cytokines secreted from TAMs. As shown in Figure 3G, overexpression of DN-IKK $\alpha$  (S176/180A) and DN-I $\kappa$ B $\alpha$  (S32/36A) reduced the inhibitory effects of TGF- $\beta$ , IL-6 and IL-1 $\beta$  on PP2Ac at the mRNA level, indicating that TAMs repressed the expression of PP2Ac through an NF- $\kappa$ B signaling pathway-dependent manner.

PP2A can repress multiple kinase signaling pathways including JNK, ERK, IKK, p38, PKC, and Src.<sup>19</sup> As IKK has been proved to be a substrate of PP2Ac, we verified whether inhibition of PP2Ac could result in the amplification of NF- $\kappa$ B pathway signaling. As shown in Figure 3H, western blot analysis confirmed that PP2A inhibitor OA treatment could phosphorylate and activate these kinase signaling pathways including JNK, ERK, IKK, p38, PKC, and Src. In addition, the expression of p-IKK was upregulated and expression of PP2Ac was downregulated after MCM treatment. However, overexpression of PP2Ac significantly attenuated the upregulation of p-IKK (Figure 3I), suggesting that TAMs repressed the expression of PP2Ac, which could further phosphorylate and activate IKK through an NF- $\kappa$ B/PP2Ac positive feedback loop.

### 3.4 | Inhibition of NF- $\kappa$ B pathway suppressed the progression of NSCLC induced by MCM treatment

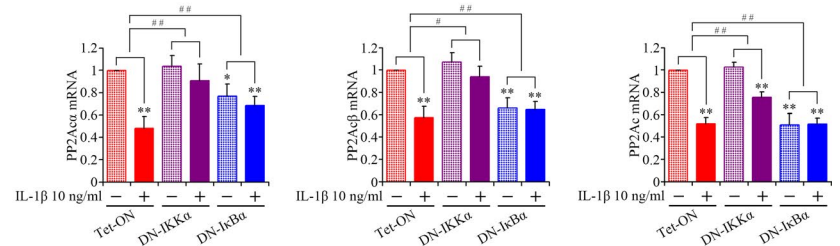
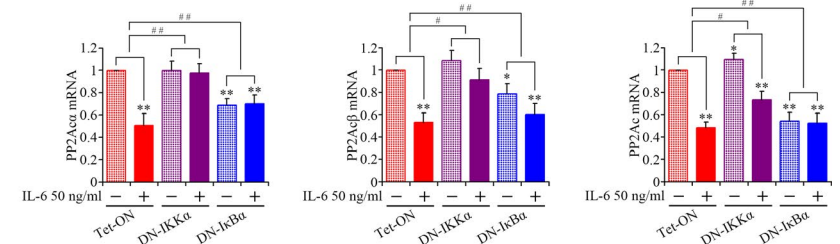
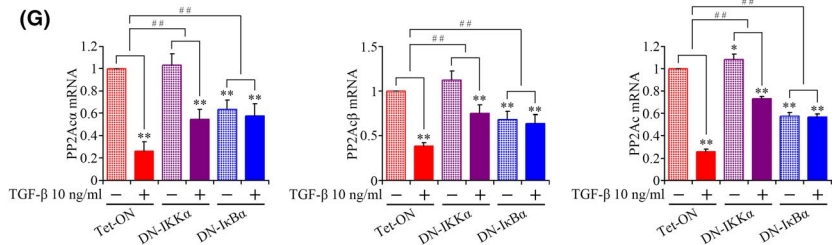
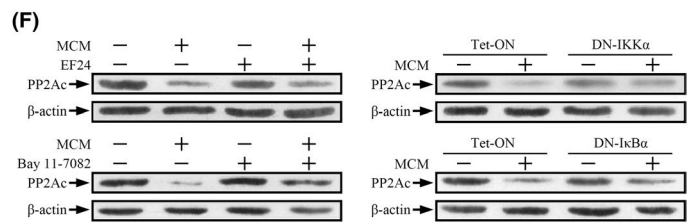
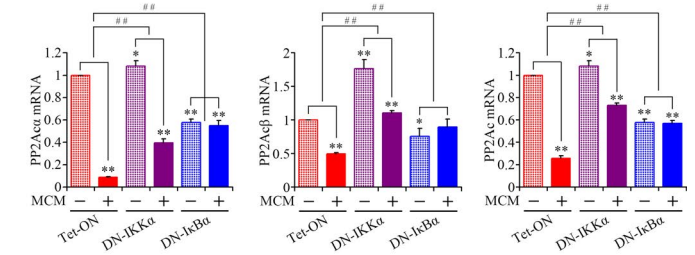
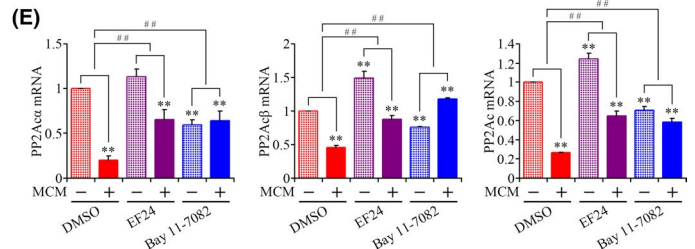
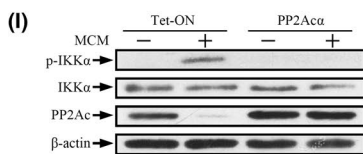
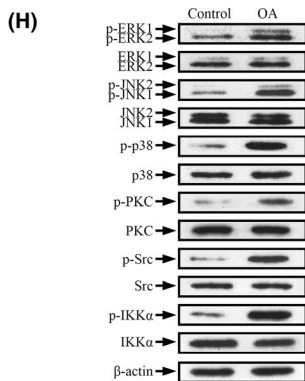
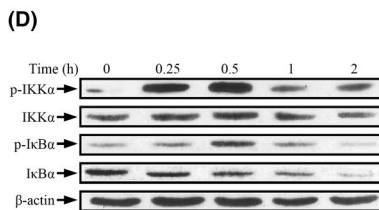
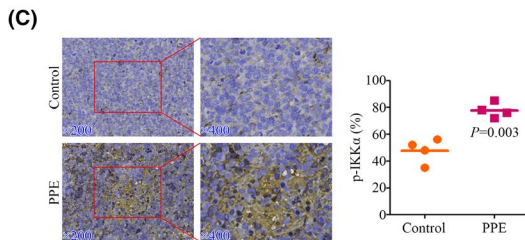
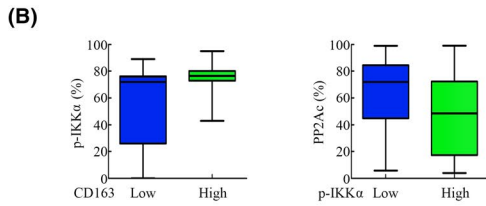
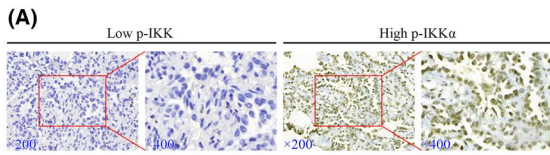
To further confirm the role of NF- $\kappa$ B pathway in the progression of lung cancer and the connections between the NF- $\kappa$ B pathway and TAMs, we constructed dominant-negative mutant forms of IKK $\alpha$  (DN-IKK $\alpha$ , S176/180A), and dominant-negative mutant forms of

I $\kappa$ B $\alpha$  (DN-I $\kappa$ B $\alpha$ , S32/36A) regulated by a lentiviral Tet-ON advanced inducible expression system. As shown in Figure 4A,B, subcutaneous xenograft nude mouse models confirmed that the growth and angiogenesis of tumors were weakened upon overexpression of DN-IKK $\alpha$  (S176/180A) and DN-I $\kappa$ B $\alpha$  (S32/36A).

In addition, we also found that overexpression of DN-IKK $\alpha$  (S176/180A) and DN-I $\kappa$ B $\alpha$  (S32/36A) impaired the proliferation and migration of lung cells induced by treatment with MCM in vitro (Figure 4C,D). These results implied that inhibition of the NF- $\kappa$ B pathway suppressed the progression of lung cancer induced by MCM treatment.

### 3.5 | CXCL1 and COL6A1 were upregulated by TAMs through NF- $\kappa$ B/PP2Ac pathway

To investigate whether NF- $\kappa$ B could regulate the expressions of downstream genes, we analyzed the microarray data of GSE44619, including 2 LUAD cancer cell lines, HCC827 and PC9, which were transduced with control retrovirus (MiG) or MiG retrovirus expressing I $\kappa$ B alpha super-repressor (SR) mutant. Using fold change (FC)  $\geq 1.5$  as the cut-off criterion, we extracted 6179 and 5841 DEGs from 2 LUAD cancer cell lines respectively. Using an available Venn diagram website, 1756 common DEGs were identified, including 792 upregulated genes and 964 downregulated genes in I $\kappa$ B alpha supersession samples compared with control samples in HCC827 and PC9 lung cancer cell lines. The overlapping areas indicated common DEGs. These DEGs identified by bioinformatics analysis might be involved in and play important roles in the NF- $\kappa$ B pathway. To further investigate the key genes between MCM treatment and the NF- $\kappa$ B pathway, we used deposited microarray datasets GSE9315 and GSE44619 mentioned above to further find the expression intersection. Four key genes including COL6A1, CXCL1, NFKB2 and RELB were found in 25 upregulated genes of MCM treatment LUAD cells sample and 964 downregulated genes of inhibitor of nuclear factor kappa B (I $\kappa$ B) alpha supersession samples. In addition, PF4 was identified in 146 downregulated genes from an MCM treatment LUAD cell sample and 792 upregulated genes from I $\kappa$ B alpha supersession samples (Figure 5A). Heat maps of the 5 genes are displayed (Figure 5B). Studies have shown that NFKB2 and RELB are involved in the nonclassical NF- $\kappa$ B pathway,<sup>31</sup> whereas CXCL1 participates in



tumor growth and angiogenesis,<sup>32-34</sup> and COL6A1 plays an important role in tumor metastasis,<sup>35</sup> implying that CXCL1 and COL6A1 might be the key downstream genes regulated by NF-κB upon treatment with MCM.

By real-time PCR, we identified that MCM treatment significantly upregulated the expression levels of CXCL1 and COL6A1, which could be attenuated upon overexpression PP2Acα, DN-IKKα(S176/180A) and DN-IκBα (S32/36A) (Figure 4C,D). We had confirmed that PP2A

**FIGURE 3** TAMs accelerated the progression of NSCLC through an NF- $\kappa$ B/PP2Ac positive feedback loop. A, Immunohistochemical examinations of p-IKK $\alpha$  levels in human NSCLC tissue samples. B, The quantitative relationships between the expression levels of p-IKK $\alpha$  and CD163/PP2Ac. \* $P < .05$  and \*\* $P < .01$  compared with the control groups. C, Immunohistochemical examination of p-IKK $\alpha$  levels in H292 orthotopic xenografts samples after treatment with PPE, and the quantitative expression levels of p-IKK $\alpha$  analyzed by SPSS. D, The protein levels of p-IKK $\alpha$ , IKK $\alpha$ , p-I $\kappa$ B $\alpha$  and I $\kappa$ B $\alpha$  in H292 cells after treatment with MCM by western blot. E, Real-time PCR showed the mRNA levels of PP2Ac $\alpha$ , PP2Ac $\beta$  and PP2Ac in H292 cells after treatment with MCM combined with NF- $\kappa$ B pathway inhibitors (EF-24 and BAY-11-7082), and upon overexpression of DN-IKK $\alpha$  (S176/180A) and DN-I $\kappa$ B $\alpha$  (S32/36A) after treatment with MCM. \* $P < .05$ , \*\* $P < .01$  and ## $P < .01$  significant differences between fold changes. F, Western blot showed the protein levels of PP2Ac $\alpha$ , PP2Ac $\beta$ , and PP2Ac in H292 cells after treatment with MCM combined with NF- $\kappa$ B pathway inhibitors (EF-24 and BAY-11-7082), and upon overexpression of DN-IKK $\alpha$  (S176/180A) and DN-I $\kappa$ B $\alpha$  (S32/36A) after treatment with MCM. G, Real-time PCR showed the mRNA levels of PP2Ac $\alpha$ , PP2Ac $\beta$  and PP2Ac in H292 cells upon overexpression of DN-IKK $\alpha$  (S176/180A) and DN-I $\kappa$ B $\alpha$  (S32/36A) after treatment with TGF- $\beta$  (10 ng/mL), IL-6 (50 ng/mL) and IL-1 $\beta$  (10 ng/mL) for 24 h. \* $P < .05$ , \*\* $P < .01$  and ## $P < .01$  significant differences between fold changes. H, Western blot showed the protein levels of p-ERK, P-JNK, p-p38, p-PKC, p-SRC, p-IKK $\alpha$ , ERK, JNK, p38, PKC, SRC and IKK $\alpha$  of H292 cells after treatment with OA (PP2A inhibitor, 30 nmol/L). I, Western blot analysis of p-IKK $\alpha$ , IKK $\alpha$  and PP2Ac protein levels in H292 cells upon overexpression of PP2Ac $\alpha$  after treatment with MCM

inhibitor OA treatment could phosphorylate and activate kinase signaling pathways including JNK, ERK, p38, IKK, PKC, and Src. MCM treatment could also inhibit PP2Ac. Therefore, we verified whether these kinase pathways participated in the upregulation of CXCL1 and COL6A1 when inhibiting PP2Ac. Lung cancer cells were first pretreated with JNK inhibitor SP600125 (20  $\mu$ mol/L), ERK inhibitor PD98059 (40  $\mu$ mol/L), p38 inhibitor Birb796 (4 nmol/L), IKK inhibitor BAY-11-7082 (10  $\mu$ mol/L), PKC inhibitor GF109203X (5  $\mu$ mol/L), and Src inhibitor PP1 (20  $\mu$ mol/L), followed by PP2A inhibitor OA (30 nmol/L) treatment. Then we detected the expression levels of CXCL1 and COL6A1 using real-time PCR. As shown in Figure 5E,F, we found that OA treatment could upregulate the expression of both CXCL1 and COL6A1. Furthermore, the inhibitors of ERK, p38, IKK, PKC, and Src significantly attenuated the upregulation of CXCL1, whereas the inhibitor of IKK significantly attenuated the upregulation of COL6A1, suggesting that these pathways may contribute to the upregulation of CXCL1 and COL6A1 upon inhibiting PP2Ac. In addition, the strong increase in luciferase after CXCL1 and COL6A1 induction by MCM could be attenuated after treatment with IKK inhibitor BAY-11-7082 (Figure 5H,I), implying that the NF- $\kappa$ B pathway may be the key regulator participating in the upregulation of CXCL1 and COL6A1 induced by TAMs through inhibiting PP2Ac.

As TAMs could activate the NF- $\kappa$ B pathway, and NF- $\kappa$ B is a transcription factor, we wondered whether NF- $\kappa$ B could directly regulate the expression of CXCL1 and COL6A1 in a promoter-dependent manner. Therefore, we identified the potential NF- $\kappa$ B binding sites in the promoter regions of CXCL1 and COL6A1 using JASPAR (<http://jaspar.genereg.net/>), as shown in Figure 5G. We then constructed luciferase reporter plasmids containing deletions of different fragment sequences to examine the direct interaction between NF- $\kappa$ B and the promoter regions of CXCL1 and COL6A1 (Figure 5D,E). The luciferase reporter assay showed that CXCL1-p-RE2 deletion significantly reduced the luciferase activity induced by MCM (Figure 5L). Furthermore, COL6A1-p-RE3 deletion significantly reduced luciferase activity (Figure 5M). Moreover, p65 participates in the formation of the NF- $\kappa$ B heterodimer and can engage cognate  $\kappa$ B enhancers. By performing ChIP assays, we validated that p65 could directly bind to CXCL1 and COL6A1 (Figure 5N,O). Taken together, these results demonstrated that NF- $\kappa$ B could interact with NF- $\kappa$ B response

elements in the CXCL1 and COL6A1 promoter, therefore inducing their transcription directly.

### 3.6 | Knockdown of COL6A1 inhibited the growth and metastasis of NSCLC

To explore the role of COL6A1 in lung cancer, RNA interference viruses were transfected into H1650 to interfere with the expression of COL6A1. Real-time PCR confirmed that expression of COL6A1 was downregulated in COL6A1 shRNA2 and COL6A1 shRNA3 (Figure 6A). By MTT and wound healing assays, we found that knockdown of COL6A1 inhibited the proliferation and migration of lung cancer cell line H1650 in vivo (Figure 6B,C). Subcutaneous xenograft nude mouse models further proved that knockdown of COL6A1 repressed the growth of lung cancer in vivo (Figure 6D). Immunohistochemistry revealed lower expression of Ki67 upon knockdown of COL6A1 compared with the control group (Figure 6E). By constructing Kaplan-Meier curves, we investigated the prognostic impact of COL6A1 on patients with NSCLC using an online website (<http://kmplot.com/analysis/>), and discovered that high expression of COL6A1 was correlated with poor OS in patients with lung cancer (Figure 6F,  $P = .0045$ ).

### 3.7 | Knockdown of CXCL1 inhibited the growth and angiogenesis of NSCLC

To further determine the role of CXCL1 in NSCLC, we also transfected H292 cells with RNA interference virus, and confirmed the expression levels of CXCL1 in each cell line (Figure 7A). Based on the interference efficiency, we selected CXCL1 shRNA 3 and CXCL1 shRNA 4 for further research. MTT showed that knockdown of CXCL1 did not affect cell proliferation in vitro (Figure 7B). However, subcutaneous xenograft nude mouse models revealed that knockdown of CXCL1 repressed the growth of lung cancer in vivo (Figure 7C). Immunohistochemistry found that downregulation of CXCL1 could also reduce the MVD of subcutaneous xenografts (Figure 7D). In addition, the HUVEC tube formation potency of

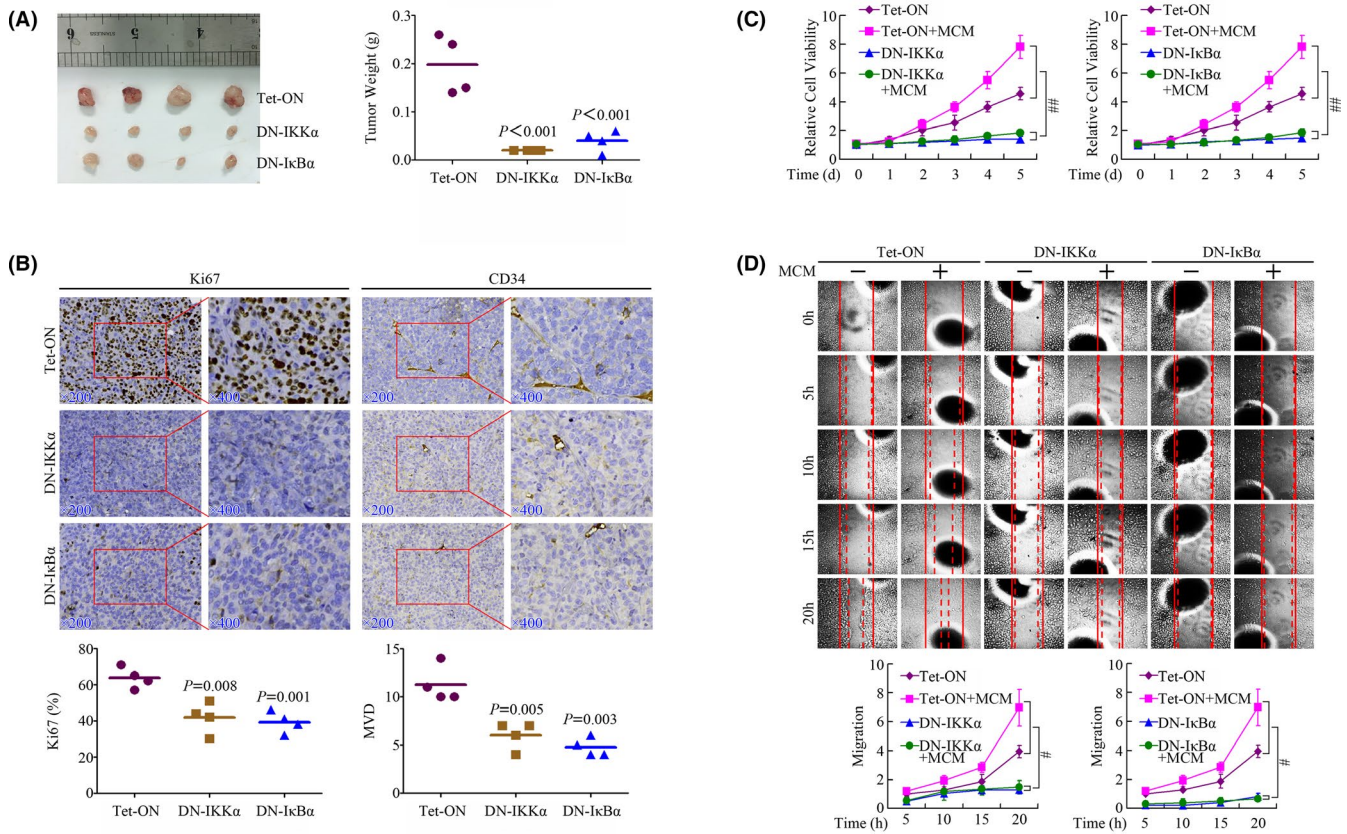


**FIGURE 4** Inhibition of NF- $\kappa$ B pathway suppressed the progression of NSCLC induced by MCM treatment. A, Photographs of subcutaneous xenografts and tumor weight in H292 DN-IKK $\alpha$  (S176/180A) and the DN-I $\kappa$ B $\alpha$  (S32/36A) overexpression group vs the control group. B, Immunohistochemical examinations of Ki67 and CD34 levels in subcutaneous xenografts samples upon overexpression of DN-IKK $\alpha$  (S176/180A) and DN-I $\kappa$ B $\alpha$  (S32/36A), and the quantitative levels of Ki67 and CD34 in each group. C, MTT confirmed that the overexpression of DN-IKK $\alpha$  (S176/180A) and DN-I $\kappa$ B $\alpha$  (S32/36A) impaired the time-dependent proliferation of H292 cells induced by MCM.  $##P < .01$  compared with the control groups. D, Wound healing assay confirmed that overexpression of DN-IKK $\alpha$  (S176/180A) and DN-I $\kappa$ B $\alpha$  (S32/36A) impaired the time-dependent inhibition on migration of H292 cells induced by MCM.  $##P < .05$  compared with the control groups

CXCL1 downregulated cells was also significantly reduced, and the potency of tube formation was rescued after adding CXCL1 (0.1  $\mu$ g/mL) to the medium (Figure 7E), indicating that knockdown of CXCL1 inhibited the angiogenesis of lung cancer induced by MCM treatment. However, the expression of CXCL1 was not correlated with OS in patients with lung cancer by Kaplan-Meier curves analysis (Figure 7F,  $P = .13$ ).

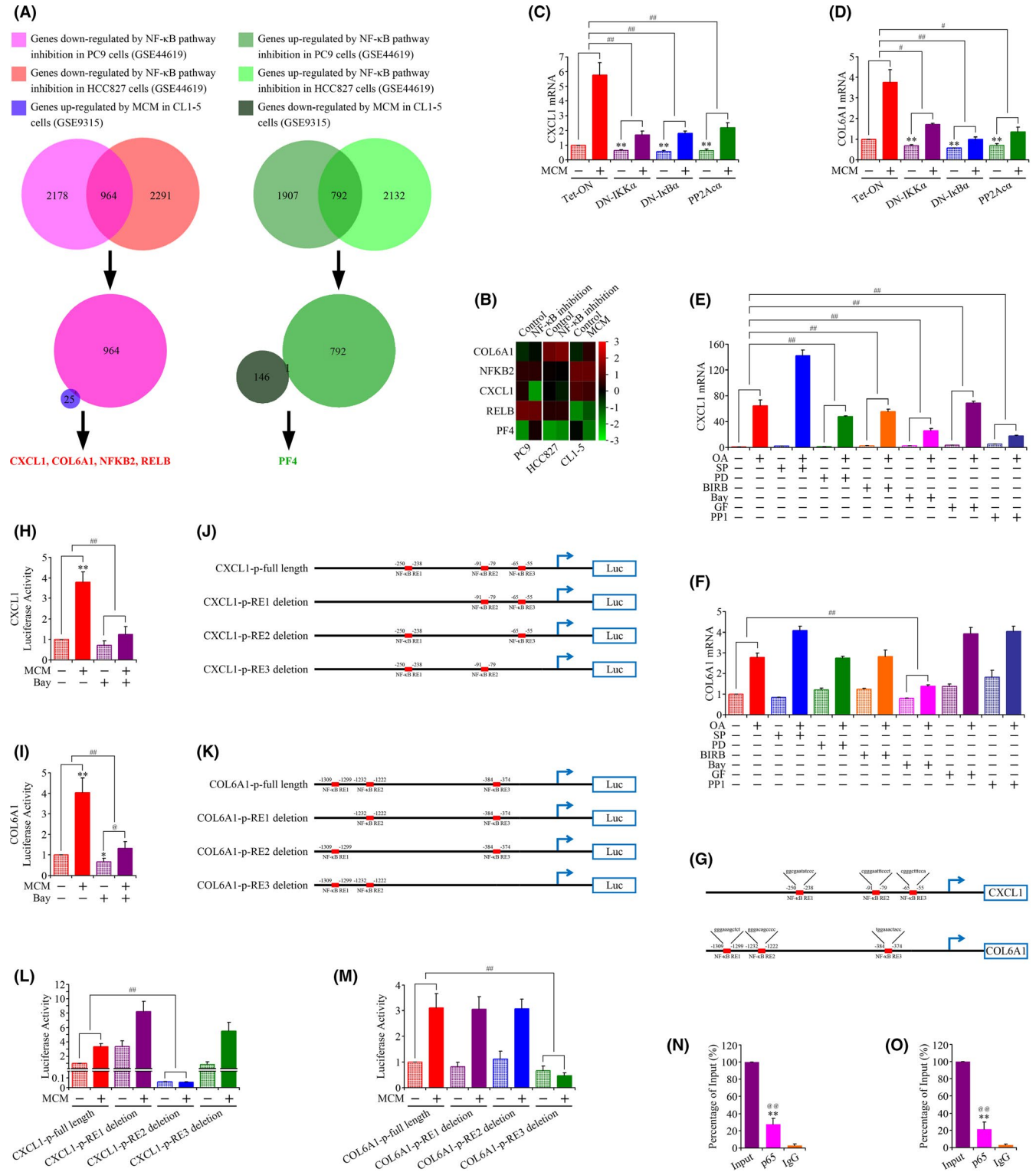
As shown in Figure 7G, the schematic diagram of the mechanism revealed that TAMs secreted cytokines TGF- $\beta$ , IL-6 and IL-1 $\beta$ , and promoted the growth and metastasis of NSCLC through an NF- $\kappa$ B/PP2Ac positive feedback loop. In addition, NF- $\kappa$ B could also induce the transcription of CXCL1 and COL6A1 by directly binding to their promoter sites, and therefore upregulate the expression of CXCL1 and COL6A1, which participated in the process of growth and metastasis of NSCLC.

**FIGURE 5** CXCL1 and COL6A1 were upregulated by TAMs through the NF- $\kappa$ B/PP2Ac pathway. A, Venn diagram analysis of differentially expressed genes (DEGs) from expression profiling datasets GSE44619 and GSE9315. B, Heatmap of the selected 5 DEGs including COL6A1, CXCL1, NFKB2, RELB, and PF4. C, D, Real-time PCR confirmed that overexpression of DN-IKK $\alpha$  (S176/180A), DN-I $\kappa$ B $\alpha$  (S32/36A) and PP2Ac $\alpha$  could all downregulate the mRNA levels of CXCL1 (C) and COL6A1 (D) in H292 cells induced by MCM.  $#P < .05$ ,  $**P < .01$  and  $##P < .01$  significant differences between fold changes. E, F, mRNA levels of CXCL1 (E) and COL6A1 (F) in H292 cells pretreated with SP600125 (JNK inhibitor, 20  $\mu$ mol/L), PD98059 (ERK inhibitor, 40  $\mu$ mol/L), BIRB796 (p38 inhibitor, 4 nmol/L), BAY-11-7082 (IKK inhibitor, 10  $\mu$ mol/L), GF109203X (PKC inhibitor, 5  $\mu$ mol/L), and PP1 (Src inhibitor, 20  $\mu$ mol/L), followed by OA (PP2A inhibitor, 30 nmol/L) treatment.  $##P < .01$  significant differences between fold changes. G, Prediction of NF- $\kappa$ B binding sites in the promoter regions of CXCL1 and COL6A1 by JASPAR. H, I, Transcriptional activity of CXCL1 (H) and COL6A1 (I) promoters after pretreatment with BAY-11-7082 (IKK inhibitor, 10  $\mu$ mol/L), followed by MCM treatment.  $*P < .05$ ,  $@P < .05$ ,  $**P < .01$  and  $##P < .01$  significant differences between fold changes. J, K, Construction of the luciferase reporter plasmids containing the deletions of different fragment sequences to examine the direct interaction between NF- $\kappa$ B and the promoter regions of CXCL1 (J) and COL6A1 (K). L, M, Transcriptional activity of CXCL1 (L) and COL6A1 (M) promoters in H292 cells transfected with luciferase reporter plasmids containing the deletions of different fragment sequences after treatment with MCM.  $##P < .01$  significant differences between fold changes. N, O, ChIP analysis showed that p65 could directly bind to CXCL1 (N) and COL6A1 (O).  $@@**P < .01$  compared with the control groups

4 | DISCUSSION

Chronic inflammation plays a crucial role in the complex progression of lung cancer.<sup>36</sup> Macrophages, as one of the major types of tumor-associated inflammatory cells, have been reported to be associated with the progression of several tumors.<sup>26</sup> Macrophages can be divided into 2 categories: type 1 or classically activated type (M1), and type 2 or alternatively activated type (M2).<sup>37</sup> M1 macrophages

appear to inhibit tumors, whereas M2 macrophages, (also known as TAMs), promote tumor invasion, metastasis, angiogenesis, and immunosuppression.<sup>16,38</sup> In this study, we identified that macrophage characteristics revealed heterogeneity in different solid cancers, and were enriched in LUAD as shown using the Cancer Immunome Database (TCIA). The infiltration of immune cellular profiles showed that macrophages were the dominant cells in the tumor micro-environment of NSCLC. Immunohistochemistry confirmed that



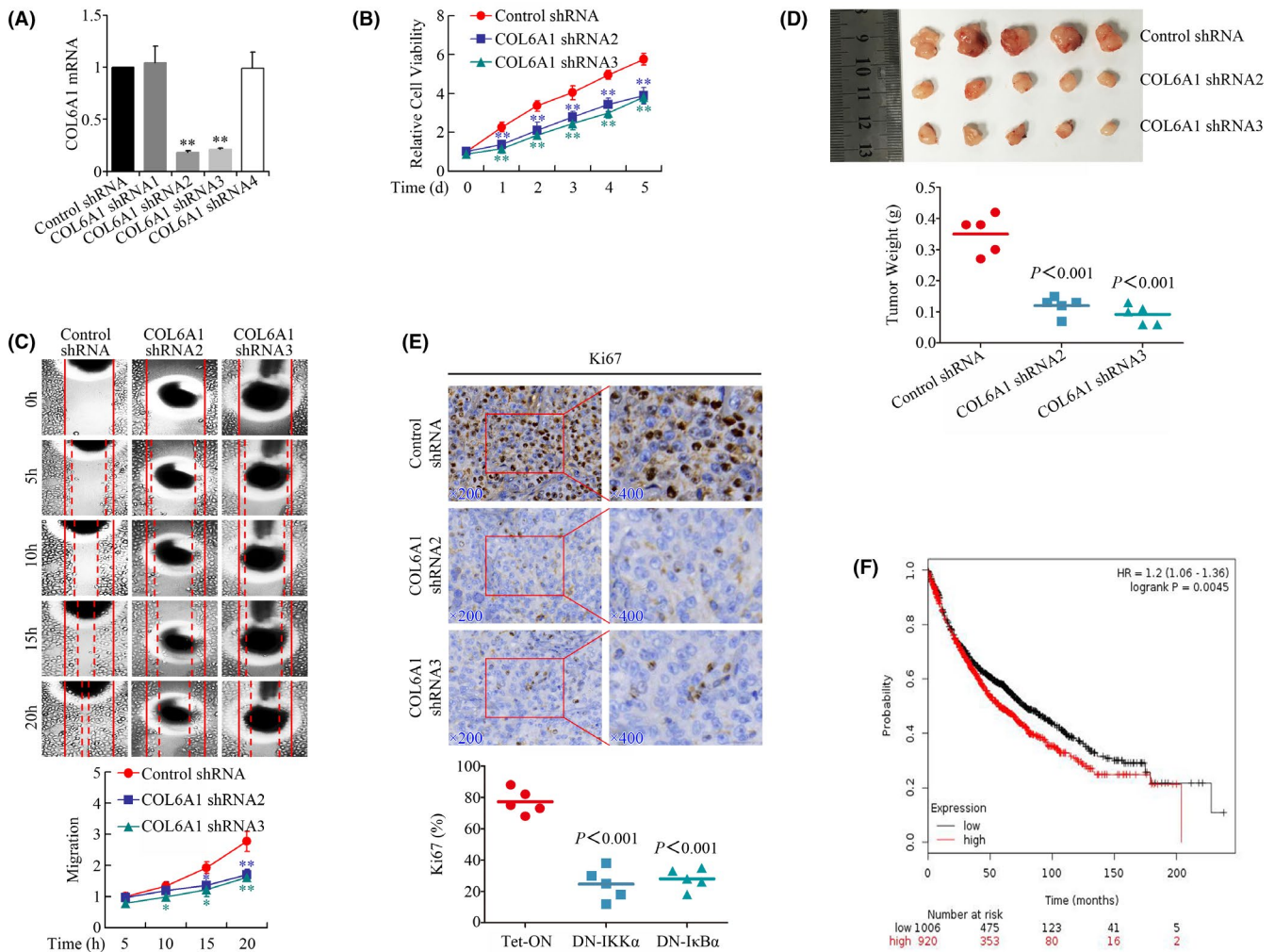


**FIGURE 6** Knockdown of COL6A1 inhibited the growth and metastasis of NSCLC. A, Confirmation of knockdown of COL6A1 in H1650 cells using real-time PCR. B, Knockdown of COL6A1 resulted in time-dependent growth inhibition on H1650 cells by MTT.  $**P < .01$  compared with the control groups. C, Knockdown of COL6A1 resulted in time-dependent inhibition on migration of H1650 cells using a wound healing assay.  $*P < .05$  and  $**P < .01$  compared with the control groups. D, Photographs of subcutaneous xenografts and tumor weight in the H1650 COL6A1 knockdown group vs the control group. E, Immunohistochemical examinations of Ki67 levels in subcutaneous xenografts samples upon knockdown of COL6A1. F, Online analysis of Kaplan-Meier curves for OS of patients with NSCLC based on COL6A1 expression

expression of CD163, a specific marker for M2, was high in most specimens from patients with lung cancer, and higher expression of CD163 indicated poorer prognosis. However, how TAMs influence lung cancer remains to be elucidated.

Based on these preliminary results, we established a nude mouse model of chronic pneumonia with PPE and an orthotopic xenograft nude mouse model, and found that tumors in the PPE group, which stimulated more infiltration of TAMs, were much larger than in the control group. Higher expression levels of CD163, Ki67 and MVD were detected in the PPE group using immunohistochemistry, indicating that TAMs could promote the growth and angiogenesis of orthotopic xenografts in vivo. Furthermore, the oncogenic effects of TAMs on proliferation and migration of lung cancer cell pretreatment with MCM have also been verified in vitro. These results were consistent with previous studies and inspired us to investigate the mechanisms involved in TAM-mediated progression of lung cancer.

Based on the microarray dataset GSE9315, which contained gene data for NSCLC cells with or without treatment with MCM, we identified 176 DEGs, and found using bioinformatics analysis that the 176 DEGs were significantly enriched in ECM-receptor interaction, P13K-Akt, TNF, TGF-beta, MAPK, NF- $\kappa$ B, and the p53 signaling pathway. Furthermore, the PPI network of DEGs showed that PP2Ac $\beta$  was downregulated notably, this was consistent with our previous study in pancreatic cancer.<sup>25</sup> PP2A is a multimeric serine/threonine phosphatase, with functions that counter-balance kinase-mediated phosphorylation throughout cell signaling networks, and response to inflammatory stimulation. PP2Ac is the catalytic subunit of PP2A and has 2 subtypes PP2Ac $\alpha$  and PP2Ac $\beta$ , sharing a common sequence of 97%. Studies have shown that PP2A is associated with the proliferation, migration and invasion of various tumors, including lung cancer.<sup>18,39-41</sup> In this study, we found that the expression of PP2Ac was negatively correlated with CD163 both

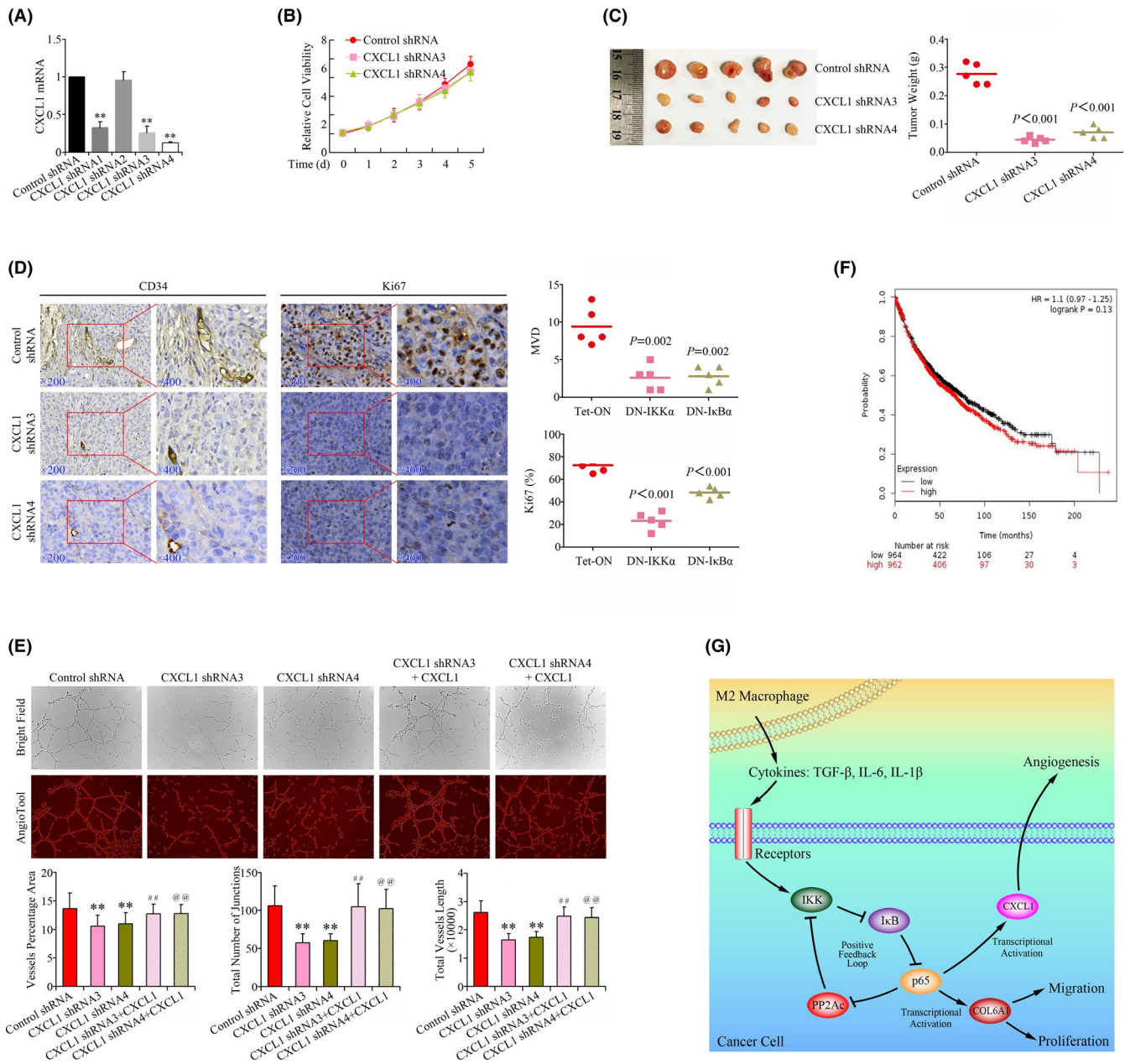


**FIGURE 7** Knockdown of CXCL1 inhibited the growth and angiogenesis of NSCLC. A, Confirmation of knockdown of CXCL1 in H292 cells using real-time PCR. B, Knockdown of CXCL1 did not affect H292 cell proliferation by MTT. C, Photographs of subcutaneous xenografts and tumor weight in the H292 CXCL1 knockdown group vs the control group. D, Immunohistochemical examination of CD34 and Ki67 levels in subcutaneous xenografts samples upon knockdown of CXCL1. E, HUVEC tube formation potency of CXCL1 downregulated cells and cells treated by adding CXCL1 (0.1  $\mu$ g/mL) to the medium. F, Online analysis of Kaplan-Meier curves for OS of patients with NSCLC based on CXCL1 expression. G, Schematic diagram of the proposed mechanism for TAMs promoting the progression of NSCLC

in specimens from patients with NSCLC and PPE-treated mice. The expression levels of PP2Ac, PP2Ac $\alpha$  and PP2Ac $\beta$  were all downregulated upon treatment with MCM, TGF- $\beta$ , IL-6, and IL-8, which are the main cytokines secreted by TAMs. Moreover, overexpression of PP2Ac markedly impaired the growth and angiogenesis of tumors in subcutaneous xenograft nude mouse models. Therefore, the pro-tumor effects of TAMs in the microenvironment of lung cancer may be executed through mechanisms involving downregulation of the expression of PP2Ac. An increasing number of studies have shown that the NF- $\kappa$ B pathway can be abnormally activated and participate

in the progression of many cancers, including lung cancer.<sup>42-45</sup> The NF- $\kappa$ B pathway also plays an important role in the expression of genes involved in inflammatory and tumors.<sup>46</sup> The activation of the canonical NF- $\kappa$ B pathway cascade mainly relies on the inducible degradation of I $\kappa$ Bs, especially I $\kappa$ B $\alpha$ , leading to the nuclear translocation of the NF- $\kappa$ B complex. Degradation of I $\kappa$ B $\alpha$  is primarily mediated by phosphorylation of I $\kappa$ B kinase (IKK), which is one of the direct substrates of PP2A.<sup>28,29,47</sup> The prototypical NF- $\kappa$ B complex is a heterodimer composed of p50 and RelA/p65. Once entering the nucleus, p65 engages cognate  $\kappa$ B enhancers, which contain one or

more  $\kappa$ B-enhancer consensus sequences and regulate the expression of downstream genes.<sup>48</sup> The canonical NF- $\kappa$ B pathway can be activated by inflammatory stimuli such as TNF- $\alpha$ , various interleukins, microbes, and virus-associated ligands.<sup>49</sup> Bioinformatics analysis revealed that the NF- $\kappa$ B pathway was also involved in the process of TAM-induced progression of lung cancer. Our data showed that the expression of p-IKK was positively related to CD163, but negatively associated with PP2Ac both in the specimens from patients with NSCLC and in PPE-treated mice. Treatment with MCM induced phosphorylation of IKK and I $\kappa$ B with a consistent abatement of the total protein levels of I $\kappa$ B, and resulted in the activation of the NF- $\kappa$ B pathway. Additionally, overexpression of DN-IKK $\alpha$  (S176/180A) and DN-I $\kappa$ B $\alpha$  (S32/36A) could impair the inhibitory effects of TAMs on PP2Ac at both mRNA and protein levels, indicating that TAMs repressed the expression of PP2Ac mainly through the NF- $\kappa$ B signaling pathway. It is worth noting that overexpression of DN-IKK $\alpha$  (S176/180A) and DN-I $\kappa$ B $\alpha$  (S32/36A) impaired the progression of lung cancer both in vitro and in vivo. Therefore, TAMs may exert a pro-tumor effect on lung cancer by inhibiting the expression of PP2Ac in a NF- $\kappa$ B signaling pathway-dependent manner.

As TAMs could activate the NF- $\kappa$ B pathway, and NF- $\kappa$ B is a transcription factor, we wondered whether NF- $\kappa$ B could directly regulate the expression of downstream genes. Four key genes, including CXCL1, COL6A1, NFKB2, and RELB, were found by further analyzed the microarray datasets GSE9315 and GSE44619, which including the gene data of 2 LUAD cancer. We also revealed that COL6A1 was associated with a poor prognosis in patients with NSCLC. Studies have shown that CXCL1 is involved in tumor growth and angiogenesis,<sup>32-34</sup> and that COL6A1 is involved in tumor metastasis,<sup>35</sup> whereas NFKB2 and RELB are mainly linked to the nonclassical NF- $\kappa$ B pathway.<sup>31</sup> As expected, we found that the expression levels of both CXCL1 and COL6A1 were increased upon treatment with MCM. Overexpression of PP2Ac $\alpha$ , DN-IKK $\alpha$  (S176/180A) and DN-I $\kappa$ B $\alpha$ (S32/36A) could attenuate the upregulation of CXCL1 and COL6A1 induced by MCM, suggesting that CXCL1 and COL6A1 could be upregulated by TAMs through an NF- $\kappa$ B/PP2Ac-dependent pathway.

CXCL1/2 is the target gene of the NF- $\kappa$ B/STAT1 pathway and studies have shown that upregulation of CXCL1 can promote the progression of liver cancer, melanoma, bladder cancer, and ovarian cancer.<sup>33,50-52</sup> COL6A1 encodes the  $\alpha$ 1 chain of collagen VI, which can regulate the cell cycle and promote tumor progression through binding to cell surface proteins and through downstream signaling cascades.<sup>53-55</sup> COL6A1 is also involved in the regulation of apoptosis, proliferation, angiogenesis, and tumor growth.<sup>56</sup> In this study, we found that knockdown of CXCL1 and COL6A1 inhibited the growth of lung cancer both in vivo and in vitro. In addition, the HUVEC tube formation potency of MCM-treated CXCL1 downregulated cells was also significantly reduced, and the potency of tube formation was rescued after adding CXCL1 (0.1 $\mu$ g/ml) to the medium. Therefore, the pro-tumor effects of TAMs on lung cancer may act by upregulating the expression of CXCL1 and COL6A1 in an NF- $\kappa$ B/PP2Ac-dependent manner.

PP2A is a repressor of several oncogenic kinase pathways, including JNK, ERK, p38, Akt, PKC, and IKK (PMID: 21958460).<sup>19</sup> Inhibition of PP2A can boost tumor growth by inducing phosphorylation and activating these oncogenic substrate kinases.<sup>29,57</sup> In this study, we verified that inhibition of PP2A by OA, a classic PP2A inhibitor, could induce phosphorylation and activate these oncogenic substrate kinases. Furthermore, inhibitors of these kinase pathways markedly attenuated the expression levels of CXCL1 and COL6A1 induced by OA, indicating that these kinase pathways may participate in the progression of lung cancer resulting from the upregulation of CXCL1 and COL6A1 through repression of PP2Ac by TAMs. Notably, TAMs could repress the expression of PP2Ac by activating the NF- $\kappa$ B pathway, whereas repression of PP2Ac could activate the NF- $\kappa$ B pathway by positive feedback.

We have mentioned that NF- $\kappa$ B is a transcription factor, we asked whether NF- $\kappa$ B could directly regulate the transcription of CXCL1 and COL6A1 in a promoter-dependent manner? We then identified potential NF- $\kappa$ B binding sites in the promoter regions of CXCL1 and COL6A1 using JASPAR (<http://jaspar.genereg.net/>). The luciferase reporter assay showed that CXCL1-p-RE2 deletion and COL6A1-p-RE3 deletion significantly reduced the luciferase activity induced by MCM. Moreover, we proved using ChIP assays that p65, the main elements of the NF- $\kappa$ B heterodimer, could directly bind to CXCL1 and COL6A1. Therefore, NF- $\kappa$ B could interact with the promoter of CXCL1 and COL6A1 directly, therefore regulating their transcription.

In summary, our study showed that TAMs promoted the metastasis and growth of NSCLC cells through an NF- $\kappa$ B/PP2Ac positive feedback loop. The NF- $\kappa$ B/PP2Ac positive feedback loop was also responsible for the progression of NSCLC resulting from the upregulation of CXCL1 and COL6A1 by TAMs. In addition, NF- $\kappa$ B could also regulate the transcription of CXCL1 and COL6A1 by directly binding to their promoter sites. Our findings provide the first evidence for how TAMs participate in the progression of NSCLC, and reveal the possibility of using NF- $\kappa$ B/PP2Ac as a therapeutic target for the treatment of NSCLC.

## ACKNOWLEDGMENTS

This work was supported by the Project of Invigorating Health Care through Science, Technology and Education, Jiangsu Provincial Medical Youth Talent (grant number QNRC2016709).

## CONFLICT OF INTEREST

The authors claim no conflicts of interest regarding the study or the manuscript.

## REFERENCES

1. Siegel RL, Miller KD, Jemal A. Cancer statistics, 2018. *CA Cancer J Clin*. 2018;68:7-30.
2. Hoffman PC, Mauer AM, Vokes EE. Lung cancer. *Lancet*. 2000;355:479-485.
3. Molina JR, Yang P, Cassivi SD, Schild SE, Adjei AA. Non-small cell lung cancer: epidemiology, risk factors, treatment, and survivorship. *Mayo Clin Proc*. 2008;83:584-594.

4. Lin WW, Karin M. A cytokine-mediated link between innate immunity, inflammation, and cancer. *J Clin Invest.* 2007;117:1175-1183.
5. Hanahan D, Weinberg RA. Hallmarks of cancer: the next generation. *Cell.* 2011;144:646-674.
6. Coussens LM, Werb Z. Inflammation and cancer. *Nature.* 2002;420:860-867.
7. Ribeiro R, Araujo A, Lopes C, Medeiros R. Immunoinflammatory mechanisms in lung cancer development: is leptin a mediator? *J Thorac Oncol.* 2007;2:105-108.
8. Aggarwal BB, Vijayalekshmi RV, Sung B. Targeting inflammatory pathways for prevention and therapy of cancer: short-term friend, long-term foe. *Clin Cancer Res.* 2009;15:425-430.
9. Shi L, Wang L, Hou J, et al. Targeting roles of inflammatory micro-environment in lung cancer and metastasis. *Cancer Metastasis Rev.* 2015;34:319-331.
10. Ben-Baruch A. Inflammation-associated immune suppression in cancer: the roles played by cytokines, chemokines and additional mediators. *Semin Cancer Biol.* 2006;16:38-52.
11. Grivennikov SI, Greten FR, Karin M. Immunity, inflammation, and cancer. *Cell.* 2010;140:883-899.
12. de Visser KE, Eichten A, Coussens LM. Paradoxical roles of the immune system during cancer development. *Nat Rev Cancer.* 2006;6:24-37.
13. Sica A, Bronte V. Altered macrophage differentiation and immune dysfunction in tumor development. *J Clin Invest.* 2007;117:1155-1166.
14. O'Callaghan DS, O'Donnell D, O'Connell F, O'Byrne KJ. The role of inflammation in the pathogenesis of non-small cell lung cancer. *J Thorac Oncol.* 2010;5:2024-2036.
15. Bremnes RM, Al-Shibli K, Donnem T, et al. The role of tumor-infiltrating immune cells and chronic inflammation at the tumor site on cancer development, progression, and prognosis: emphasis on non-small cell lung cancer. *J Thorac Oncol.* 2011;6:824-833.
16. Zumsteg A, Christofori G. Corrupt policemen: inflammatory cells promote tumor angiogenesis. *Curr Opin Oncol.* 2009;21:60-70.
17. Coffelt SB, Hughes R, Lewis CE. Tumor-associated macrophages: effectors of angiogenesis and tumor progression. *Biochim Biophys Acta.* 2009;1796:11-18.
18. Li W, Chen Z, Zong Y, et al. PP2A inhibitors induce apoptosis in pancreatic cancer cell line PANC-1 through persistent phosphorylation of IKK $\alpha$  and sustained activation of the NF- $\kappa$ B pathway. *Cancer Lett.* 2011;304:117-127.
19. Li W, Chen Z, Gong F-R, et al. Growth of the pancreatic cancer cell line PANC-1 is inhibited by protein phosphatase 2A inhibitors through overactivation of the c-Jun N-terminal kinase pathway. *Eur J Cancer.* 2011;47:2654-2664.
20. Charoentong P, Finotello F, Angelova M, et al. Pan-cancer immunogenomic analyses reveal genotype-immunophenotype relationships and predictors of response to checkpoint blockade. *Cell Rep.* 2017;18:248-262.
21. Reinartz S, Schumann T, Finkernagel F, et al. Mixed-polarization phenotype of ascites-associated macrophages in human ovarian carcinoma: correlation of CD163 expression, cytokine levels and early relapse. *Int J Cancer.* 2014;134:32-42.
22. Lütjhe L, Raupach T, Michels H, et al. Exercise intolerance and systemic manifestations of pulmonary emphysema in a mouse model. *Respir Res.* 2009;10:7.
23. Kurimoto E, Miyahara N, Kanehiro A, et al. IL-17A is essential to the development of elastase-induced pulmonary inflammation and emphysema in mice. *Respir Res.* 2013;14:5.
24. Sujak E. Hospital treatment of psychiatric complications of epilepsy. *Psychiatr Pol.* 1973;7:681-682.
25. Tao M, et al. Inflammatory stimuli promote growth and invasion of pancreatic cancer cells through NF- $\kappa$ B pathway dependent repression of PP2Ac. *Cell Cycle.* 2016;15:381-393.
26. Zhu J, Zhi Q, Zhou BP, Tao M, Liu J, Li W. The role of tumor associated macrophages in the tumor microenvironment: mechanism and functions. *Anticancer Agents Med Chem.* 2016;16:1133-1141.
27. Arino J, Woon CW, Brautigam DL, Miller TB Jr, Johnson GL. Human liver phosphatase 2A: cDNA and amino acid sequence of two catalytic subunit isoforms. *Proc Natl Acad Sci USA.* 1988;85:4252-4256.
28. DiDonato JA, Hayakawa M, Rothwarf DM, Zandi E, Karin M. A cytokine-responsive I $\kappa$ B kinase that activates the transcription factor NF- $\kappa$ B. *Nature.* 1997;388:548-554.
29. Millward TA, Zolnierowicz S, Hemmings BA. Regulation of protein kinase cascades by protein phosphatase 2A. *Trends Biochem Sci.* 1999;24:186-191.
30. Inoue J, Gohda J, Akiyama T, Semba K. NF- $\kappa$ B activation in development and progression of cancer. *Cancer Sci.* 2007;98:268-274.
31. Sun SC. Non-canonical NF- $\kappa$ B signaling pathway. *Cell Res.* 2011;21:71-85.
32. Wang D, Sai J, Carter G, Sachatzidis A, Lolis E, Richmond A. PAK1 kinase is required for CXCL1-induced chemotaxis. *Biochemistry.* 2002;41:7100-7107.
33. Cao Z, Fu B, Deng B, Zeng Y, Wan X, Qu L. Overexpression of Chemokine (C-X-C) ligand 1 (CXCL1) associated with tumor progression and poor prognosis in hepatocellular carcinoma. *Cancer Cell Int.* 2014;14:86.
34. Dhawan P, Richmond A. Role of CXCL1 in tumorigenesis of melanoma. *J Leukoc Biol.* 2002;72:9-18.
35. Chiu KH, Chang YH, Wu YS, Lee SH, Liao PC. Quantitative secretome analysis reveals that COL6A1 is a metastasis-associated protein using stacking gel-aided purification combined with iTRAQ labeling. *J Proteome Res.* 2011;10:1110-1125.
36. Xu Y, et al. Curcumin inhibits tumor proliferation induced by neutrophil elastase through the upregulation of alpha1-antitrypsin in lung cancer. *Mol Oncol.* 2012;6:405-417.
37. Gordon S. Alternative activation of macrophages. *Nat Rev Immunol.* 2003;3:23-35.
38. Riabov V, Gudima A, Wang N, Mickley A, Orekhov A, Kzhyshkowska J. Role of tumor associated macrophages in tumor angiogenesis and lymphangiogenesis. *Front Physiol.* 2014;5:75.
39. Ito A, et al. A truncated isoform of the PP2A B56 subunit promotes cell motility through paxillin phosphorylation. *EMBO J.* 2000;19:562-571.
40. Jackson J, et al. Protein phosphatase-2A associates with the cytoskeleton to maintain cell spreading and reduced motility of nonmetastatic Lewis lung carcinoma cells: the loss of this regulatory control in metastatic cells. *Invasion Metastasis.* 1997;17:199-209.
41. Meisinger J, Patel S, Vellody K, et al. Protein phosphatase-2A association with microtubules and its role in restricting the invasiveness of human head and neck squamous cell carcinoma cells. *Cancer Lett.* 1997;111:87-95.
42. Keshk WA, Zineldeen DH, Wasfy RE, El-Khadrawy OH. Fatty acid synthase/oxidized low-density lipoprotein as metabolic oncogenes linking obesity to colon cancer via NF- $\kappa$ B in Egyptians. *Med Oncol.* 2014;31:192.
43. Yang MH, et al. KML001 inhibits cell proliferation and invasion in pancreatic cancer cells through suppression of NF- $\kappa$ B and VEGF-C. *Anticancer Res.* 2014;34:3469-3474.
44. Nakshatri H, Bhat-Nakshatri P, Martin DA, Goulet RJ Jr, Sledge GW Jr. Constitutive activation of NF- $\kappa$ B during progression of breast cancer to hormone-independent growth. *Mol Cell Biol.* 1997;17:3629-3639.
45. DiDonato JA, Mercurio F, Karin M. NF- $\kappa$ B and the link between inflammation and cancer. *Immunol Rev.* 2012;246:379-400.
46. Karin M. Nuclear factor- $\kappa$ B in cancer development and progression. *Nature.* 2006;441:431-436.
47. Vallabhapurapu S, Karin M. Regulation and function of NF- $\kappa$ B transcription factors in the immune system. *Annu Rev Immunol.* 2009;27:693-733.

48. Chen LF, Greene WC. Shaping the nuclear action of NF-kappaB. *Nat Rev Mol Cell Biol.* 2004;5:392-401.
49. Smits H, van Beelen A, Hesse C, et al. Commensal Gram-negative bacteria prime human dendritic cells for enhanced IL-23 and IL-27 expression and enhanced Th1 development. *Eur J Immunol.* 2004;34:1371-1380.
50. Amiri KI, Richmond A. Fine tuning the transcriptional regulation of the CXCL1 chemokine. *Prog Nucleic Acid Res Mol Biol.* 2003;74:1-36.
51. Kawanishi H, Matsui Y, Ito M, et al. Secreted CXCL1 is a potential mediator and marker of the tumor invasion of bladder cancer. *Clin Cancer Res.* 2008;14:2579-2587.
52. Bolitho C, Hahn MA, Baxter RC, Marsh DJ. The chemokine CXCL1 induces proliferation in epithelial ovarian cancer cells by transactivation of the epidermal growth factor receptor. *Endocr Relat Cancer.* 2010;17:929-940.
53. Cheng IH, Lin Y-C, Hwang E, et al. Collagen VI protects against neuronal apoptosis elicited by ultraviolet irradiation via an Akt/phosphatidylinositol 3-kinase signaling pathway. *Neuroscience.* 2011;183:178-188.
54. Lampe AK, Zou Y, Sudano D, et al. Exon skipping mutations in collagen VI are common and are predictive for severity and inheritance. *Hum Mutat.* 2008;29:809-822.
55. Bonnemann CG. The collagen VI-related myopathies Ullrich congenital muscular dystrophy and Bethlem myopathy. *Handb Clin Neurol.* 2011;101:81-96.
56. Zhu YP, Wan FN, Shen YJ, Wang HK, Zhang GM, Ye DW. Reactive stroma component COL6A1 is upregulated in castration-resistant prostate cancer and promotes tumor growth. *Oncotarget.* 2015;6:14488-14496.
57. Janssens V, Goris J, Van Hoof C. PP2A: the expected tumor suppressor. *Curr Opin Genet Dev.* 2005;15:34-41.

#### SUPPORTING INFORMATION

Additional supporting information may be found online in the Supporting Information section.

**How to cite this article:** Liang Z-W, Ge X-X, Xu M-D, et al. Tumor-associated macrophages promote the metastasis and growth of non-small-cell lung cancer cells through NF- $\kappa$ B/PP2Ac positive feedback loop. *Cancer Sci.* 2021;112:2140-2157. <https://doi.org/10.1111/cas.14863>